Journal of Rock Mechanics and Geotechnical Engineering. 2011, 3 (1): 30–38

Journal of Rock Mechanics and Geotechnical Engineering

Journal online: www.rockgeotech.org

Laboratory tests and numerical simulations of brittle marble and squeezing schist at Jinping II hydropower station, China

Chunsheng Zhang*, Weijiang Chu, Ning Liu, Yongsheng Zhu, Jing Hou

East China Investigation and Design Institute, China Hydropower Engineering Consulting Group Co., Hangzhou, 310014, China

Received 1 January 2011; *received in revised form 5 February 2011*; *accepted 16 February 2011*

Abstract: Four 16.7 km-long tunnels with diameters ranging from 12.4 to 14.6 m are now under construction at Jinping II hydropower station along the Yalong River. The tunnels pass through Triassic rocks below Jinping Mountain. The tunnels are characterized with high overburden, long alignment and complex geological conditions. Brittle failure in marble and squeezing in schist are the primary problems in tunnelling. This paper introduces the studies of laboratory tests on Jinping II marble as well as numerical prediction of excavation damaged zone (EDZ) of tunnel section in brittle marble and determination of reinforced concrete lining thickness for restraining time-dependent deformation in the schist tunnel section. Laboratory tests indicate that Jinping II marble presents a complex brittle-ductile-plastic transition behavior of post-peak response with increasing confining pressure. Such behavior can be described numerically with the Hoek-Brown model. The EDZ was calibrated and predicted using both fast Lagrangian analysis of continua (FLAC) and particle flow code (PFC). The predicted result of EDZ in sections with different qualities of rock mass under various overburden pressures is quite helpful in understanding EDZ characterization and support design. A power-law creep model was used to support the lining design, especially in determining the lining thickness. Field convergence measurement data over 19 months were used to calibrate the creep model properties, followed by a sensibility analysis of reinforced concrete lining thickness that was launched to present the maximum lining compressive stress.

Key words: deep tunnel; time-dependent behavior; excavation damaged zone (EDZ); squeezing; marble

1 Introduction

Jinping II hydropower station (Jinping II project) is located at the Yalong River in Liangshan Autonomous Region, Sichuan Province, China. The Jinping II project will have 8 generators, each with a capacity of 600 MW, making a total capacity of 4 800 MW. The expected annual electricity generation will be over 24.2 TW·h. It is the largest hydropower station along the Yalong River.

The sluice gate of the Jinping II project is located at Maomaotan in the west of Jinping Mountain and the plant in the east at Dahuigou. The four headrace tunnels, each about 16.7 km in length running parallel to and crossing the Jinping Mountain, an alpine karst zone, will connect the sluice gate and the plant units. The four headrace tunnels are numbered from No.1 to No.4 (Fig.1) (the information from construction would be helpful for headrace tunnels excavation). The headrace tunnels No.1 and No.3 are mainly excavated by tunnel boring machine (TBM, Fig.2), while the headrace tunnels No.2 and No.4 are excavated by drill and blast method.

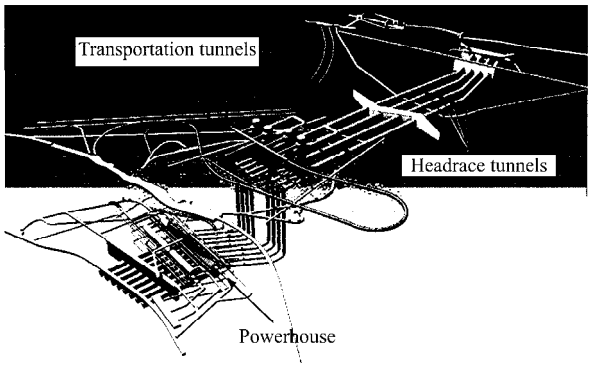

Fig.1 Layout of main hydraulic facilities of Jinping II project.

The diameters of the headrace tunnels range from 12.4 to 14.6 m. The construction of the headrace tunnels No.2 and No.4 started in December 2006, and the headrace tunnels No.1 and No.3 started in October 2008. The headrace tunnel No.1 will be completed in July 2011 at schedule.

The two transportation tunnels running parallel to the headrace tunnels were excavated in November 2003 and completed on August 8, 2008. The diameters

Doi: 10.3724/SP.J.1235.2011.00030
*Corresponding author. Tel: +86-571-56738306;
E-mail: zhang_cs@ecidi.com
Support by the China Postdoctor Fund (20100471757)

Fig.2 TBMs used in tunnel excavation (the left one is Robins TBM for the headrace tunnel No.1 and the right one is Herrenknecht TBM for the headrace tunnel No.2).

of the transportation tunnels range from 5.5 to 6.25 m. The transportation tunnels serve as not only traffic and transport access but also exploratory adit, test adit and construction adit for the headrace tunnels.

A dewater tunnel running parallel to the headrace tunnels with a diameter of 7.2 m was excavated mainly by TBM. The dewater tunnel lies between the headrace tunnels and the transportation tunnels.

1.1 Geology of the tunnel route

Jinping Mountain consists of a series of complex folds, and the rocks along the tunnels belong to the Triassic period, 205–250 million years old. A simplified geological section in Fig.3 shows the location of the rock type along the headrace tunnels. The rocks along the tunnels are mostly metamorphic rocks. The strike of the rocks is generally NS to NNE-SSW with steep dip angles. The main rocks are marble, which occupies large part of groups T_{2b}, T_{2y} and T_{2z}. The rock group T_{2b} is located in the middle core of Jinping Mountain. Another rock is schist, which is mainly the typical squeezing rock, and occupies several hundred meters in each headrace tunnel.

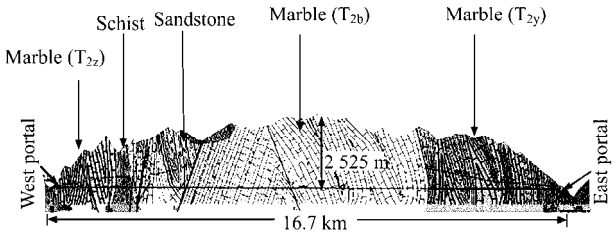

Fig.3 Simplified geological profile along the headrace tunnel No.1.

Most faults encountered during tunnel construction are mainly with steep dip angle. Their thicknesses are from 1 cm to 5 m and mainly between 0.1 and 0.5 m. Joints with strikes of NE and NW are the most common rock structures along the transportation tunnels. Most joints are described to be closed.

A series of laboratory tests were carried out to investigate the strength of rock samples. The uniaxial compressive strength (UCS) of marble samples is quite discrete and varies from 80 to 170 MPa. The UCS of dry schist ranges from 35 to 40 MPa, and that of saturated schist samples ranges from 18 to 22 MPa. The marble is hard and brittle, and the schist is soft and ductile.

1.2 Key problems in tunnelling

The average overburden depth of the Jinping tunnels is 1 500–2 000 m, and the maximum is 2 525 m. The tunnels are characterized by long alignment, high overburden, high groundwater pressure and complex geological conditions. Therefore, proper and effective methods should be adopted to solve the key technical problems, such as spalling and rockburst in hard rock, squeezing deformation in schist tunnel section, etc..

The rockburst is severe in the construction of the transportation tunnels and the dewater tunnel. Destress blasting was used to control the strainbursts. In practice, destress blasting was very helpful in those three tunnels construction. The frequency and intensity of rockburst in the headrace tunnels are apparently lower than those in the transportation tunnels and the dewater tunnel. The possible reasons are as follows: (1) the rockburst, especially the strainburst, is scale-related, and different opening scales will result in different rockburst risks; and (2) the quality and time of rock support in the headrace tunnels are better than those in the transportation tunnels.

In this paper, particular attention is paid to the determination of EDZ in brittle marble tunnel section and the thickness of reinforced concrete lining in squeezing tunnel such as schist section. In order to understand the brittle failure of marble, a series of axial and biaxial compression tests with acoustic emission (AE) monitoring were carried out, and the results of those tests were also presented in the paper.

2 Laboratory tests on marble

2.1 Damage evolution in brittle rock

The failure process of brittle rock on laboratory scale has been extensively studied [1–6]. AE monitoring on rock sample during compression tests plays an important role in crack study with different load levels. Basically, the stress-strain curve of a brittle rock sample, such as granite, could be divided into four phases: (1) crack closure phase (I); (2) linear elasticity phase (II); (3) stable crack growth phase (III); and (4) unstable crack growth phase (IV). Figure 4 shows the

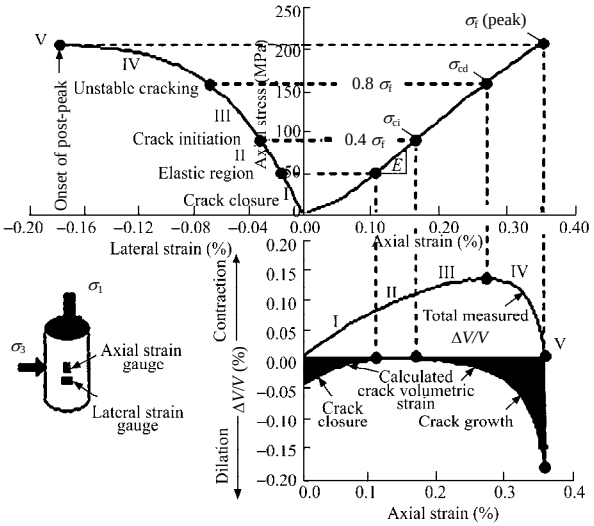

Fig.4 Stress-strain curves obtained from a single uniaxial compression test on Lac du Bonnet granite [4].

definitions of crack initiation stress (σ_{ci}), crack damage stress (σ_{cd}) and peak strength (σ_f). The crack initiation stress, σ_{ci}, is defined as the stress level marking the onset of dilation and the beginning of phase III where the stress-strain curve is deviated from linear-elastic behavior, indicating the development and growth of stable cracks. These cracks are referred to stable cracks since an increase in load is required to raise further cracking, and time-dependent crack growth does not occur under a constant load. The crack damage stress, σ_{cd}, is defined as the stress level marking the beginning of phase IV, where the reversal of volumetric strain curve occurs, indicating that the dilation due to the formation and growth of cracks exceeds the elastic compression of the rock resulting from increasing load [4]. Loading a sample with stress above σ_{cd} results in time-dependent increases in damage to the material, leading to an ultimate sample failure under a sustained constant load. The crack damage stress, therefore, is believed to be indicative of the long-term strength of the rock [7].

2.2 Compression test on Jinping marble

In general, more than sixty marble specimens were tested to obtain the values of σ_{ci}, σ_{cd} and *UCS*. Figure 5 shows typical test results on T_{2b} specimen. The compression tests were conducted on MTS-815 rock mechanics test system. In order to capture the crack growth in rock specimens, the AE sensors were employed to record the AE events during loading. In addition, the liner variable differential transducers were used to measure the axial deformation, and the circumferential deformation was measured by an extensometer.

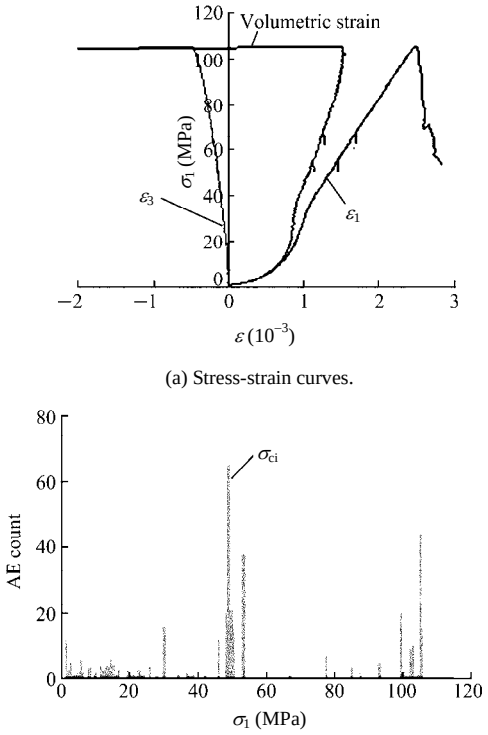

(a) Stress-strain curves.

(b) Axial stress-AE count relation.

Fig.5 Typical results of axial compression test and AE monitoring on marble of group T_{2b} (where σ_1 is the axial stress, ε_1 is the axial strain, and ε_3 is the lateral strain) [8].

Figure 5 shows that the AE count increases significantly when the axial stress reaches 47 MPa and the UCS of the specimen is 105 MPa. The stress threshold of crack initiation stress (σ_{ci}) is 45% of UCS. The crack damage threshold (σ_{cd}) is defined as the inflection point of the volumetric strain-axial stress curve. Unfortunately, it is hard to identify the inflection point of the volumetric strain curve from Fig.5. Based on the experimental results on sixty specimens, some conclusions are drawn as follows: (1) the crack initiation stress threshold is 40%–55% of UCS; (2) the crack damage threshold is 80%–90% of UCS; and (3) the marble T_{2b} has higher UCS than other group marbles in Jinping II project. The UCS of marble T_{2b} ranges from around 100 to 160 MPa, but that of marble T_{2y} ranges from 80 to 140 MPa.

Comparison of experimental results of σ_{ci}/UCS and σ_{cd}/UCS of Lac du Bonnet granite in an underground research laboratory (URL) in Canada indicates that the dimensionless crack initiation threshold and dimensionless crack damage threshold are rather the same.

Triaxial compression tests were also carried out on Jinping marble [8]. The size of specimens is 50 mm in diameter and 100 mm in height. The confining pressure ranges from 2 to 50 MPa. Figure 6 presents

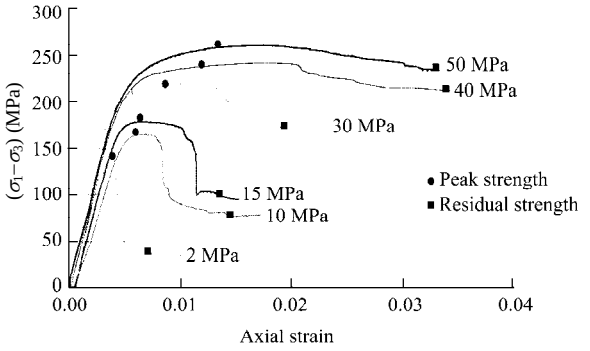

Fig.6 Results of triaxial test for marble T_{2b} in Jinping II project.

the test results of stress-strain curves under different confining pressures. The characterization of post-peak curves is strongly affected by the confining pressure. Under a low confining pressure, the curve rapidly drops down to a residual strength after reaching the peak strength, showing a typical brittle behavior. Increasing the confining pressure, for example, up to 15 MPa, the curve does not drop down immediately after reaching its peak strength. Instead, the curve remains at the peak value for a period of time before dropping down. The stress-strain curves show an apparently ductile material behavior under high confining pressures. When the confining pressure increases to 50 MPa, the peak strength is close to the residual one, and the stress-strain curve shows a plastic material behavior.

Similar to the test results of marble T_{2b}, the laboratory test results of groups T_{2y}^4 and T_{2y}^5 also reveal the brittle-ductile-plastic transition behavior with increasing confining pressure.

2.3 Long-term loading test on Jinping marble

If the stress level in laboratory test is kept constant, i.e. the stress level is larger than the crack initiation threshold, the specimen would eventually fail. The time-dependent behavior of rock can be characterized by performing a series of static-fatigue tests to produce a time-to-failure curve [7].

The static-fatigue test consists of two operational stages: initial loading stage and constant loading stage. In the initial loading stage, the specimen is axially loaded to a constant. The constant loading stage is determined according to the laboratory test results of crack initiation threshold. The axial load is set as a constant value until the specimen fails.

In the static-fatigue tests, environmental conditions of moisture and temperature were held constant. The axial stress σ_1, the confining pressure P_c and the time-to-failure t_f were all recorded. The axial load at failure during a short-term compression test is denoted as σ_f. The stress difference maintained during a static-fatigue test conducted at a confining pressure P_c is $\sigma = \sigma_1 - P_c$. The stress difference at failure during a short-term test is $\sigma_c = \sigma_1 - P_c$. To facilitate comparison between different data sets, Potyondy [9] suggested a static-fatigue curve by plotting the logarithm of the time-to-failure, t_f, versus the driving stress-ratio given by $\sigma / \sigma_c = (\sigma_1 - P_c) / (\sigma_f - P_c)$. The peak strength σ_f is confirmed in uniaxial or triaxial compression tests performed before the static-fatigue test. Schmidtke and Lajtai [10] suggested that the failure process should be fitted by exponential equation.

The static-fatigue tests were carried out to investigate the static-fatigue limit of Jinping marble. Based on the exponential equation fitting, it is obtained that the static-fatigue limit is 0.48 for marble T_{2y}^5, as shown in Fig.7.

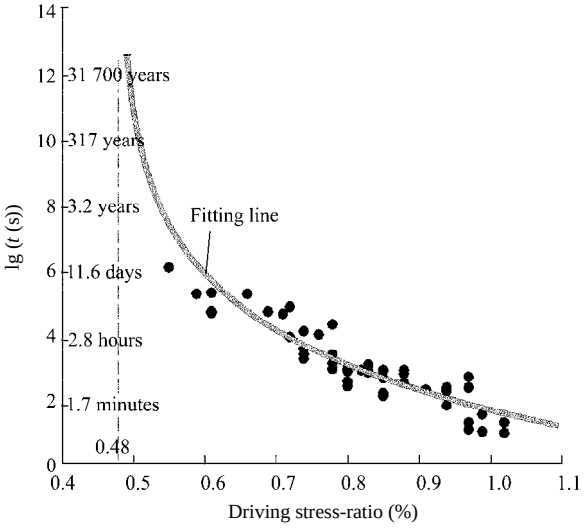

Fig.7 Static-fatigue test data for marble group T_{2y}^5 with exponential fitting.

The static-fatigue test of Jinping marble presented in this paper is under uniaxial compression condition, further laboratory tests with different confining pressures are ongoing.

3 Prediction of EDZ

The in-situ rock mass properties and behaviors around the underground opening would change due to stress redistribution, blasting, moistness and temperature variation, etc.. Knowledge of the degree and extent of the EDZ is important for the design and construction of Jinping deep tunnels. EDZ could be mechanically unstable, which in turn requires a rock support system. EDZ could also form a permeable pathway for groundwater flow, which would threaten

the safety of Jinping deep tunnels [11].

Both fast Lagrangian analysis of continua (FLAC) and particle flow code (PFC) were used for the calibration of the ground EDZ profile measurement, followed by prediction of the maximum EDZ depth in different tunnel sections. The prediction results are helpful for support design.

3.1 Description of brittle-ductile-plastic transition behavior of Jinping marble

The Hoek-Brown model was used to describe the brittle-ductile-plastic transition behavior of Jinping marble. The EDZ depth of the headrace tunnels was predicted after model calibration. The technical details of the Hoek-Brown model properties for describing the brittle-ductile-plasticity were put forward by Zhang et al. [8]. The model response of brittle-ductile-plastic transition is shown in Fig.8(a), and the Hoek-Brown envelopes of peak and residual strengths are also shown in Fig.8(b). It can be observed that the numerical results duplicate the brittle-ductile-plastic transition with the increasing confining pressure obtained from laboratory test. In Fig.8(a), as the confining pressure increases to 30 MPa, the ductile response will turn into a perfect-plastic response, while under low confining pressures, for example, $\sigma_3 = 0$ or 5 MPa, the stress-strain curve drops down immediately before it reaches the peak strength. The difference between the peak and the residual strengths decreases with the increasing confining pressure. This character can also be reproduced in numerical simulations.

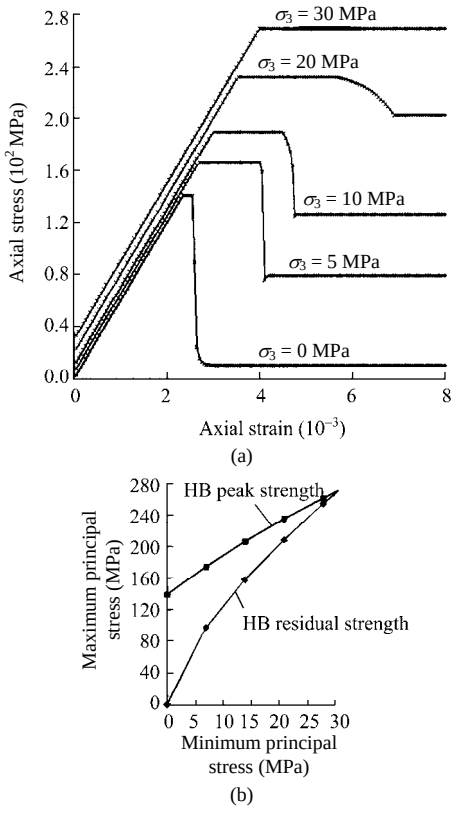

Fig.8 Description of marble brittle-ductile-plastic transition behavior with different confining pressures.

Figure 9 presents the numerical results of stress path near the headrace tunnel opening. The rock mass quality in simulations is of typical class II (*GSI* = 70) according to the geological strength index (*GSI*). The peak strength of the Hoek-Brown model is obtained from the Hoek-Brown experimental strength criterion (*UCS* = 140 MPa, *GSI* = 70, m_i = 9, m_i is the Hoek-Brown constant for marble), and the residual strength of rock mass in the tunnel section is back calculated based on the measured ground EDZ profile.

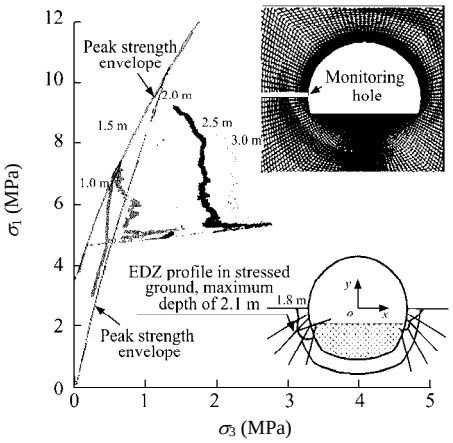

Fig.9 Measured EDZ profile on the headrace tunnel section and numerical calibration (the overburden depth is about 1 733 m).

Figure 9 also shows the calibration of post-peak behavior with the Hoek-Brown model. The right-hand side in Fig.9 presents the measured EDZ profile at the two toe corners of the tunnel. The measured depth of EDZ at the left corner ranges from 1.8 to 2.1 m.

The curves in the left side of Fig.9 represent simulated stress paths at the locations of monitoring hole with different depths from the opening. The stress path at the location 1 m deep from the opening shows a typical brittle response and severe damage, and stress path at this depth reaches residual strength envelope. The stress path at the location of 2.0 m at depth has not touched, but is close to the peak strength envelope. Thus, the thickness of model-referred EDZ is in the range of 1.5 and 2.0 m along the horizontal hole in the left toe area, which is consistent with the measurement.

3.2 Predicting EDZ depth with the Hoek-Brown model

According to the calibrations mentioned above, the post-peak properties of the Hoek-Brown model can be

obtained. If the in-situ stress of numerical simulations is set with different overburdens, the EDZ depths of different tunnel sections can be easily obtained.

The prediction of EDZ in tunnel sections with different overburdens was performed under typical ground conditions (rock mass class II, *GSI* = 70). Table 1 shows the prediction results of the maximum EDZ depth of the headrace tunnels. The numerical results are helpful for support design, especially for the determination of the length of rock bolts.

Table 1 The EDZ profile prediction of rock class II under different depths by FLAC^{3D}.

Depth (m)	EDZ depth (m)
1 500	2.2
1 800	2.6
2 000	3.0
2 200	3.3

At the depths of 1 800 to 2 200 m from ground surface, the maximum EDZ of rock class II predicted by the Hoke-Brown model is 3.3 m. According to the principle that bolts should cover the damaged zone of surrounding rock, the length of system bolts is 4.5 m at least. Accounting for time-dependent character of EDZ in deep tunnels, the rock bolt of 6 m in length was selected in the tunnel section with an overburden over 1 800 m.

3.3 Predicting EDZ profile using PFC

The EDZ is associated with crack initiation and propagation. Some numerical researches focus on the simulations of crack initiation and propagation directly. Since the research by Griffith, many subsequent researchers have been using shearing or sliding crack to model the initiation of brittle failure [12, 13]. When using the Hoek-Brown model to calibrate parameters for relatively poor ground rock mass of class III with *GSI* = 55, it has been found that the model always intends to overestimate the depth of EDZ. This finding leads to the application of PFC to prediction of EDZ. The bonded particle model based PFC provides a numerical method that can reproduce qualitatively almost every mechanical mechanism and phenomenon that occurs in rocks, although adjustments and modifications are needed to obtain quantitative matches in model property [14]. This model also has been used for calibration and prediction of EDZ under poor ground conditions of Jinping II project.

The numerical calibration was performed by comparison of simulated EDZ and field measurement. Figure 10 shows a simulated EDZ profile of TBM excavated headrace tunnel section, which is well

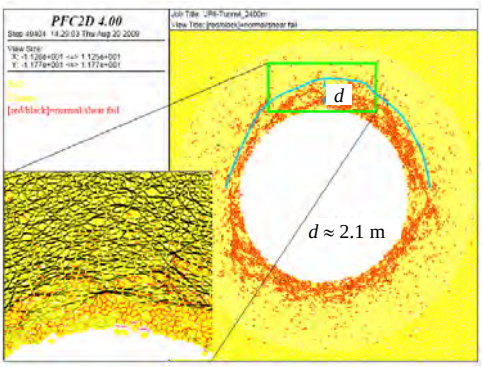

Fig.10 EDZ profile simulated by PFC (the overburden is 1 500 m).

consistent with the field measurement.

Table 2 shows the prediction of the maximum EDZ depth in tunnel sections with different overburdens.

Table 2 Prediction of the EDZ profile under unfavorable ground conditions in TBM excavated headrace tunnel (*GSI* = 55).

Depth (m)	EDZ depth (m)
1 350	1.9
1 500	2.1
1 800	2.3
2 000	2.7
2 200	3.2

Apparently, both the Hoek-Brown model based on FLAC and the bonded particle model based on PFC have the same capability to deal with the EDZ prediction.

4 Determination of lining thickness in squeezing tunnel section

Predicting the long-term behaviors of underground structures is not an easy task, as it needs a reliable constitutive model, which can interpret the measurement of viscous phenomena [15]. Because of scale effect, the rock rheological property measured on the samples in the laboratory cannot be extrapolated directly to field scale. It is necessary to calibrate numerical results with in-situ measurement over a long period of time.

The headrace tunnels in Jinping II project can be divided into hard rock and squeezing rock tunnel sections. Each headrace tunnel consists of a schist section of several hundred meters in length. It is anticipated that tunnelling in the schist, will be particularly difficult since the rocks are weak and may give rise to squeezing ground. In this context, particular attentions are paid to the determination of reinforced concrete lining thickness and lining

installation time, using measured convergence data.

4.1 Time-dependent model

In-situ deformation and convergence rate, extend of the creep zone around the tunnel, and squeezing load on support system in weak rock tunnel depend on many factors such as rock types, rock mass characteristics, in-situ stresses, groundwater, excavation and lining construction sequence, relative stiffness between lining and ground around the opening, and delay in support installation [16]. In order to estimate ground deformation and support loads, different approaches were presented. Many researchers attempted to use rock mass classification system (empirical approach) to predict the squeezing pressure [17]. Numerical simulation based on different creep models was usually adopted to predict field squeezing.

In this paper, a power-law viscoplastic model was used to predict lining pressure and ground convergence over a long period of time. The power-law model combines the behavior of the viscoelastic two-component Norton power law and the Mohr-Coulomb elastoplastic model. The total strain rate is decomposed into three components:

$$\dot{\varepsilon} = \dot{\varepsilon}_{ij}^{\mathrm{e}} + \dot{\varepsilon}_{ij}^{\mathrm{p}} + \dot{\varepsilon}_{ij}^{\mathrm{c}} \tag{1}$$

where $\dot{\varepsilon}$ is the total strain rate; $\dot{\varepsilon}_{ij}^{\mathrm{e}}$ is the elastic strain rate; $\dot{\varepsilon}_{ij}^{\mathrm{p}}$ is the plastic strain rate; $\dot{\varepsilon}_{ij}^{\mathrm{c}}$ is the viscous strain rate, which is definite as

$$\dot{\varepsilon}_{ij}^{\mathrm{c}} = \dot{\varepsilon}_{\mathrm{cr}} \frac{\partial q}{\partial S_{ij}} \tag{2}$$

where q is the von Mises stress, $q = \sqrt{\frac{3}{2} S_{ij} S_{ij}}$; S_{ij} is the stress deviatoric tensor; $\dot{\varepsilon}_{\mathrm{cr}}$ can be written as

$$\dot{\varepsilon}_{\mathrm{cr}} = \dot{\varepsilon}_{\mathrm{cr}}^{1} + \dot{\varepsilon}_{\mathrm{cr}}^{2} \tag{3}$$

where

$$\dot{\varepsilon}_{\mathrm{cr}}^{1} = \begin{cases} A_1 q^{n_1} & (q \geq \sigma_1^{\mathrm{ref}}) \\ 0 & (q < \sigma_1^{\mathrm{ref}}) \end{cases} \tag{4a}$$

$$\dot{\varepsilon}_{\mathrm{cr}}^{2} = \begin{cases} A_2 q^{n_2} & (q \leq \sigma_2^{\mathrm{ref}}) \\ 0 & (q > \sigma_2^{\mathrm{ref}}) \end{cases} \tag{4b}$$

where A_1, n_1, A_2, n_2, σ_1^{ref} and σ_2^{ref} are the model parameters.

4.2 Comparison of in-situ convergence measurement with numerical results

The first step of time-dependent behavior analysis is to determine model viscous parameters. The proper viscous parameters can be obtained for the model by matching numerical simulation results and field measurement through back analysis. The initiation point of creep deformation needs to be selected before back analysis. It is not easy to be found out when the elastic and plastic deformations are completed and the creep deformation is initiated, for the durations of elastic and plastic deformations are associated with rock types, rock mass characteristics and in-situ stresses. In a common sense, the elastic and plastic deformations maybe last several weeks in hard rock tunnels, and several months in squeezing tunnels. The convergence monitoring data in schist tunnel show that the deformation of stable convergence section lasts for more than 6 months, averagely up to 8–9 months. It can be concluded that the period of elastic and plastic deformations is at least 6 months.

In this back analysis, the convergence measurement section of kilometric point (KP), KP(1)1+675, was selected as a typical section, and the squeezing deformation in this section was considerably large. It is assumed that the creep deformation starts at 6 months after excavation. The shotcrete lining with 30 cm thick, rock bolt with 6–9 m in length and steel arch with a clear spacing of 100 cm were considered after the tunnel was excavated. The convergence measurement of line *BC* on section KP(1)1+675 is 19.16 mm in a period of 13 months after creep deformation initiation, and the average convergence rate is 0.049 mm per day.

We assume that $\sigma_1^{\mathrm{ref}} = \sigma_2^{\mathrm{ref}} = 0$ in back analysis using power-law viscoplastic model, and the number of model parameters is reduced to two (A_1 and n_1).

Figure 11 shows the measured ground deformation and numerical results in a period of 1.1 years after creep deformation initiation (6 months after tunnel excavation). From Fig.11, the following conclusions can be drawn: (1) the simplified power-law model well duplicates the ground convergence, and the back analysis model parameters are $A_1 = 1.8\mathrm{e}^{-21}$ and $n_1 = 9.0$; and (2) the convergence deformation curves

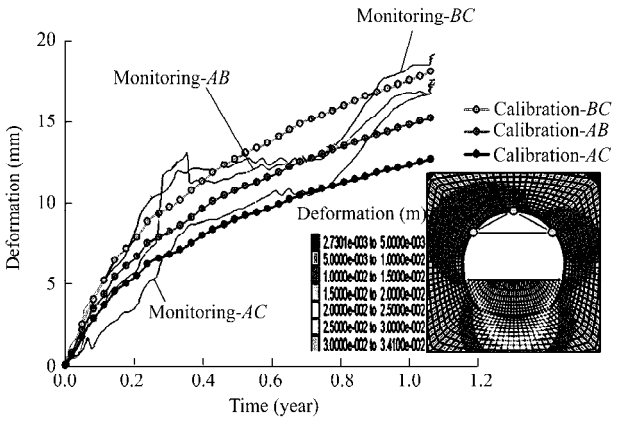

Fig.11 Measured deformations of ground and numerical simulated results for tunnel section KP(1)1+675.

show a nonlinear characterization. The convergence rate is significant in the first stage, decreasing after the support is adopted for one year. It is anticipated that the reinforced concrete lining will be subjected to squeezing due to the rock mass creep deformation.

4.3 Prediction of reinforced concrete lining pressure

There are two advantages for the installation of reinforced concrete lining in the schist tunnel section of Jinping II project. The reinforced concrete lining could restrain time-dependent convergence, and protect the schist from water inrush induced by rock mass softening when the headrace tunnel is under operation. The determination of the thickness of reinforced concrete lining and the timely lining installation are associated with time-dependent deformation behavior of rocks. The well calibrated creep model parameters are helpful in predicting the compressive stress increment with time after the reinforced concrete lining is installed.

Table 3 presents the sensibility analyses of reinforced concrete lining thickness (0.6, 0.8, 1.5 and 2.0 m) and lining installation periods (1.5 and 2 years after excavation). The time-dependent compressive stress of reinforced concrete lining is extrapolated over a period of approximate 80 years based on the calibrated creep model parameters.

Table 3 Prediction of the compressive stress of reinforced concrete lining after installation based on the well calibrated creep model parameters.

Lining installation period (year)	Time (year)	Maximum compressive stress in lining (MPa)			
		0.6 m	0.8 m	1.5 m	2.0 m
1.5	2	6	6	4	4
	4	12	11	9	8
	6	16	15	12	11
	8	19	18	14	12
	10	21	20	15	13
	20	27	25	19	17
	30	31	29	22	19
	40	34	31	23	20
	50	36	33	24	21
	60	38	35	25	22
	70	39	36	26	23
	80	40	37	27	24
2.0	2	2	1	2	1
	4	9	7	6	6
	6	13	12	10	9
	8	16	15	11	10
	10	18	16	13	12
	20	25	23	17	15
	30	29	26	20	17
	40	31	29	21	19
	50	34	30	23	20
	60	35	32	24	21
	70	37	33	25	21
	80	38	34	25	22

The concrete used for reinforced lining in schist section in Jinping II project is labelled as $C30_{90}W8$, whose compression strength is around 20.1 MPa. It is suggested from Table 3 that the thickness of reinforced concrete lining should be 1.5–2.0 m when considering the lining operation over 50 years. The convergence measurement in KP(1)1+675 is one of the most significant monitoring item. The prediction based on the convergence measurement data may overestimate the creep deformations against other sections. The initiation time of creep deformation also impacts the prediction results, and the exact determination time is difficult or even unrealistic. Considering these factors comprehensively, 1.5 m in thickness of reinforced lining is acceptable.

5 Conclusions

The tunnels in Jinping II project are characterized by large overburden depth, long alignment and complex geological conditions. The excavation-induced damages in marble tunnel section and squeezing deformation in schist tunnel section are the typical issues in Jinping II project. Based on laboratory tests and numerical simulations, the following conclusions are drawn:

(1) The crack initiation threshold stress (σ_{ci}) of Jinping II marble is 40%–55% of UCS, and the crack damage threshold stress (σ_{cd}) is 80%–90% of UCS. The dimensionless threshold stresses mentioned above are closed to Lac du Bonnet granite's laboratory test results, so it can be concluded that the brittle property of Jinping II marble is similar to that of Lac du Bonnet granite under low confining pressures. The information is helpful in understanding the brittle failure of surrounding opening in Jinping tunnels.

(2) The static-fatigue limit of marble group T_{2y}^{5} is 0.48 based on the static-fatigue laboratory test. The information is helpful in understanding the time-dependent degradation near opening, resulting in fracture propagation over time-dependency behavior of strength.

(3) A brittle-ductile-plastic transition behavior with increasing confining pressure has been presented based on the laboratory test results of Jinping II marble. This behavior can be numerically reproduced with the Hoek-Brown model.

(4) The Hoek-Brown model based on FLAC and the bonded model based on PFC were used to calibrate the field EDZ measurement for model properties.

Prediction of EDZ profile and the maximum damage depth was proposed on different rock masses with various overburdens, and both the Hoek-Brown model and the bonded particle model were used in EDZ prediction. The predicted EDZ result is useful in support design.

(5) The tunneling conditions in the schist tunnel section are unfavourable because of squeezing and creep deformation. In order to restrain creep deformation in schist section and prevent schist softening during headrace tunnel operation, a reinforced concrete lining is needed for schist tunnel section.

(6) A power-law creep model was used to support the lining design, especially in determining lining thickness. Field convergence measurement data over 19 months were used to calibrate the creep model properties, followed by sensibility analyses of reinforced concrete lining thickness and installation time to obtain the maximum compressive stress of lining.

Acknowledgments

The authors gratefully acknowledge the supports from Ertan Hydropower Development Company, Itasca Consulting China Ltd., and Institute of Rock and Soil Mechanics, Chinese Academy of Sciences.

References

[1] Bieniawski Z T. Mechanism of brittle fracture of rock: parts I—theory of the fracture process. International Journal of Rock Mechanics and Mining Sciences and Geomechanics Abstracts, 1967, 4 (4): 395–404.

[2] Bieniawski Z T. Mechanism of brittle fracture of rock: parts II—experimental studies. International Journal of Rock Mechanics and Mining Sciences and Geomechanics Abstracts, 1967, 4 (4): 407–408.

[3] Bieniawski Z T. Mechanism of brittle fracture of rock: parts III—fracture in tension and under long-term loading. International Journal of Rock Mechanics and Mining Sciences and Geomechanics Abstracts, 1967, 4 (4): 425–426.

[4] Martin C D, Chandler N A. The progressive fracture of Lac du Bonnet granite. International Journal of Rock Mechanics and Mining Sciences and Geomechanics Abstracts, 1994, 31 (6): 643–659.

[5] Cai M, Kaiser P K, Tasaka Y, et al. Generalized crack initiation and crack damage stress thresholds of brittle rock masses near underground excavations. International Journal of Rock Mechanics and Mining Sciences, 2004, 41 (5): 833–847.

[6] Martin C D. The strength of massive Lac du Bonnet granite around underground openings. PhD Thesis. Winnipeg: University of Manitoba, 1993.

[7] Lau J S O, Chandler N A. Innovative laboratory testing. International Journal of Rock Mechanics and Mining Sciences, 2004, 41 (8): 1 427–1 445.

[8] Zhang Chunsheng, Chen Xiangrong, Hou Jing, et al. Study of mechanical behavior of deep-buried marble at Jinping II hydropower station. Chinese Journal of Rock Mechanics and Engineering, 2010, 29 (10): 1 999–2 009 (in Chinese).

[9] Potyondy D O. Simulating stress corrosion with a bonded-particle model for rock. International Journal of Rock Mechanics and Mining Sciences, 2007, 44 (5): 677–691.

[10] Schmidtke R H, Lajtai E Z. The long-term strength of Lac du Bonnet granite. International Journal of Rock Mechanics and Mining Sciences and Geomechanics Abstracts, 1985, 22 (6): 461–465.

[11] Cai M, Kaiser P K. Assessment of excavation damaged zone using a micromechanics model. Tunnelling and Underground Space Technology, 2005, 20 (4): 301–310.

[12] Horii H, Nemat-Nasser S. Brittle failure in compression: splitting, faulting and brittle ductile transition. Philosophical Transactions of the Royal Society of London (A, Mathematical and Physical Sciences), 1986, 319 (3): 337–374.

[13] Lajtai E Z, Carter B J, Ayari M L. Criteria for brittle fracture in compression. Engineering Fracture Mechanics, 1990, 37 (1): 59–74.

[14] Potyondy D O, Cundall P A. A bonded-particle model for rock. International Journal of Rock Mechanics and Mining Sciences, 2004, 41 (8):1 329–1 364.

[15] Boidy E, Bouvard A, Pellet F. Back analysis of time-dependent behavior of a test gallery in clay stone. Tunnelling and Underground Space Technology, 2002, 17 (4): 415–424.

[16] Shalabi F I. FE analysis of time-dependent behavior of tunneling in squeezing ground using two different creep models. Tunnelling and Underground Space Technology, 2005, 20 (3): 271–279.

[17] Barton N R, Lien R, Lunde J. Engineering classification of rock masses for the design of tunnel support. Rock Mechanics and Rock Engineering, 1974, 6 (4): 189–236.